Journal of Inorganic Biochemistry 199 (2019) 110725

Contents lists available at ScienceDirect

Journal of Inorganic Biochemistry

journal homepage: www.elsevier.com/locate/jinorgbio

Computational studies, design and synthesis of Pd(II)-based complexes: Allosteric inhibitors of the Human Topoisomerase-IIα

Fillipe V. Rocha[a,*,1], Renan L. Farias[b,1], Mauro A. Lima[a], Victor S. Batista[c], Nailton M. Nascimento-Júnior[c], Saulo S. Garrido[d], Andréia M. Leopoldino[e], Renata N. Goto[e], Adriano B. Oliveira[f], Johannes Beck[g], Christian Landvogt[g], Antônio E. Mauro[b], Adelino V.G. Netto[b]

[a] UFSCar – Univ Federal de São Carlos, Departamento de Química, São Carlos, Brazil
[b] UNESP – Univ Estadual Paulista, Instituto de Química, Departamento de Química Geral e Inorgânica, Araraquara, Brazil
[c] UNESP – Univ Estadual Paulista, Instituto de Química, Departamento de Química Orgânica, Araraquara, Brazil
[d] UNESP – Univ Estadual Paulista, Instituto de Química, Departamento de Bioquímica e Tecnologia Química, Araraquara, Brazil
[e] USP – Univ de São Paulo, Department of Clinical Analyses, Toxicology and Food Sciences, Ribeirão Preto, Brazil
[f] UFS – Univ Federal de Sergipe, Departamento de Química, São Cristóvão, Brazil
[g] Rheinische Friedrich-Wilhelms-Universität Bonn, Institut für Anorganische Chemie, Bonn, Germany

A B S T R A C T

Herein, a robust docking protocol was developed by using a low-cost workflow to highlight the modulation at ATPase domain from Human Topoisomerase-IIα (TOP2A) towards four novel Pd(II)-complexes bearing *N*,*S*-donor ligands. In vitro TOP2A inhibition assay confirmed the ability of them to prevent the enzyme functions into concentration ranging at 6.25–25 μM. These results exhibited more effectivity than anticancer agent etoposide (35 μM) and merbarone (40–50 μM). The compounds were screened via Resazurin assay against MCF-7, MDA-MB-231 (Human breast), DU-145 (Human prostate), A549 (Human lung) and Cal27 (Human tongue) tumor cell lines revealing great cytotoxic effects, primarily to MCF-7 (IC_{50} = 1.81–4.46 μM). As well, **1–4** exhibited their selectivity index (SI) higher than cisplatin against HEK-293 (human kidney) normal cells, at least 11.6-fold (SI_{1-4} = 1.4–5.0; SI_{cis} = 0.12). Further, Red Blood Cell hemolytic test suggested in vitro non-toxic character for compound **4**, previously evaluated as the most effective TOP2A inhibitor.

1. Introduction

The Topoisomerase-IIα (TOP2A) enzyme may modulate the chromosomal DNA topology being required for replication and chromosome segregation [1,2]. In the enzymatic cycle, the entwined DNA strands are disentangled by an ATP hydrolysis-dependent strand-passage mechanism. Since TOP2A expression is significantly elevated in proliferating cells and some types of cancer cells, it has been used as a biomarker and clinically targeted by anticancer agents, notably etoposide and doxorubicin [3]. The TOP2A inhibitors are sorted into two classes: (1) poisons, whose mechanism of inhibition makes an increase in the level of TOP2A-DNA cleavage complex and (2) catalytic inhibitors, which are able to inhibit the enzyme without the establishment of the above-mentioned complex [1–4].

Despite several TOP2A poisons have been reported in the preclinical phase, their non-selective inhibition towards TOP2B isoform has triggered cardiotoxicity adverse effect [5]. Such drawback has inspired the development of new catalytic inhibitors more selective than poisons. In this context, there has been an increasing interest in new TOP2A inhibitors based on metal-based complexes. Among them, square-planar copper compounds displayed an inhibition mechanism involving the interruption of ATP hydrolysis [6-8].

Recently, we have reported the inhibition of TOP2A functions induced by cationic square-planar palladium(II) complexes bearing thiosemicarbazide (TCZ) as *N*,*S*-donor ligand [9]. These compounds were more cytotoxic than cisplatin against MCF-7 cell line (human breast epithelial adenocarcinoma) and inhibited TOP2A activity at 5–25 μM. Interestingly, these complexes have not induced any inhibitory effects towards TOP1 (ATP non-dependent) in DNA relaxation assays suggesting a possible role as catalytic TOP2A inhibitors via prevention of the ATP hydrolysis [9]. These findings have stimulated us to elaborate an in silico methodology to explore the interplay between enzyme and Pd(II) complexes into the ATPase domain of the TOP2A.

For this purpose, we have chosen the homodimer form of the TOP2A (PDB ID: 1ZXM) [10], whose crystal structure was solved at 1.87 Å and shown a co-crystalized adenosine-5′-(b,c-imido)triphosphate (ANP), a

* Corresponding author.
E-mail address: fillipe@ufscar.br (F.V. Rocha).
[1] These authors contributed equally to this work.

https://doi.org/10.1016/j.jinorgbio.2019.110725
Received 8 February 2019; Received in revised form 20 May 2019; Accepted 27 May 2019
Available online 06 June 2019
0162-0134/

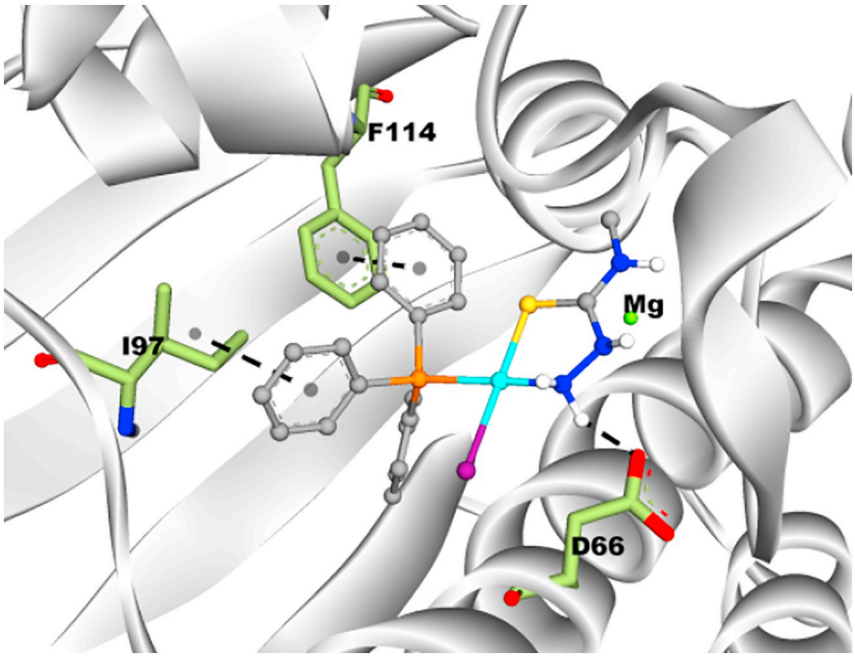

Fig. 1. Docking pose of hit-ligand in the ANP pocket (PDB ID: 1ZXM). ATPase domain is represented as a cartoon. Side chains of key-residues are indicated as O (red), N (blue) and C (green) sticks. Hit-ligand is represented as C (grey), P (orange), I (purple), N (blue), S (yellow), Pd (cyan). Non-polar H-atoms and non-interacting residues were omitted for clarity.

non-hydrolysed ATP analogue, embedded in the ATP pocket. After that, the molecular docking calculation for the structurally characterized [PdI(TCZ)(PPh_3)]I (FIO7, hit-ligand) [9] has been evaluated in *N*-terminal domain (Fig. 1). See ESI for more details.

As result of the simulation, FI07 found suitable conformation in the ANP binding site, as expected from our previous in vitro results [9]. The highest score (37.25), calculated through the ChemPLP scoring function, has given rise a pose where triphenylphosphine (PPh_3) ligand takes part in the intermolecular recognition through π-π stack and σ-π contacts with the side chains of F114 and I97, respectively. Also, the thiosemicarbazide ligand establishes electrostatic hydrogen bonding interaction with the side chain of D66. Even though there have been favourable interactions between hit-ligand and ANP cavity, the molecular scaffold of the FI07 inhibitor has not filled the ATP pocket efficiently.

In this context, we have explored a molecular hybridization approach to design new square-planar Pd(II) complexes aiming at improving: (a) molecular recognition into ATPase domain and (b) cytotoxic activity efficiency. Take into account to predict in vitro selectivity index (SI), comparative cytotoxicity features against HEK-293 normal cell line were assessed. Finally, to support the safety uses for the most promising metallodrug candidate, in vitro toxicology profile was performed out by means of Red Blood Cell (RBC) hemolytic test.

2. Results and discussion

2.1. Design of the *1–4* inhibitors

The first step intended at replacing the TCZ by a thiosemicarbazone (TSC) ligand derived from cinnamaldehyde. We hypothesized that incorporating a cinnamaldehyde fragment at the coordinated *N*-atom (Fig. 2b) would result in a more potent inhibitory effect by optimizing interactions with the hydrophobic pocket. Recently, a TSC containing cinnamaldehyde moiety showed an improvement on TOP2A inhibitory and antiproliferative activities upon coordination to Ni(II) and Cu(II) metal centres (3.2–5.9 μM) [11]. Also, taken into account the importance of H-donor groups for molecular recognition, the *N*(4)-thiocarbamide position was preserved without substituent groups. Likewise, the triphenylphosphine ligand (PPh_3) was also maintained since the Pd-PPh_3 moiety of the hit-molecule interacts favourably with the hydrophobic pocket. Finally, to complete the four-fold coordination sphere around the Pd(II) metal centre, monodentate ligands have been used (Fig. 2).

All molecular structures for designed inhibitors were optimized by using the semi-empirical method PM7 [12]. The root-mean-square deviation (RMSD) retrieved from overlay between compound **2** and its experimental molecular crystal structure accounts to 0.5387 Å and confirms the quality of the geometry optimization (Fig. S1). See ESI for more details.

2.2. Molecular docking evaluation

Minimized 3-D protein structure from original 1ZXM.pdb exhibited a Ramachandran plot with 734 (98.3%) residues at favourable torsion angles. Further 11 (1.5%) at allowed and 2 (0.3%) at outlier regions (Fig. S2). Using the chain-A, the overall model quality for final protein structure have been assessed via Z-score, which supports the suitability of that for desired simulation (Fig. S3). Additionally, FTSite and FTMap (computational mapping servers) exposed both precise biding-site position and regions of the surface with major contributions to the ligand-binding free energy, respectively [13]. Accordingly, it is observed that the ATPase domain is split into two subunits with different polar affinities. The hydrophobic and hydrophilic pockets are individually highlighted as blue and green (Fig. 3).

A rigid docking simulation by using GOLD software v5.5 [14] was performed out. To evaluate the accuracy of the protocol, the crystallized ligand ANP was re-docked into the ATP pocket. This control molecule with the highest ChemPLP score (135.36) retrieved similar atomic positions in agreement with the crystal (RMSD = 0.588 Å). For molecular recognition, modelled ANP ligand kept up in contact with similar side chains of residues N91, N120, S148, S149, N150, R162, N163, G164, Y165, G166, A167, K168, Q376 and K378 compatible with PDB*sum* (see, ESI Fig. S4).

The ATPase domain from TOP2A conserves the nucleotide binding site characteristic from GHKL superfamily (Histidine kinase, DNA gyrase B and HSP90 ATPase domains) [3,10,15–17]. As a result of the simulation, **1–4** had different binding mode profiles than hit-ligand. Interestingly, these compounds modulated the *N*-terminal strap of the dimer-related protomer (B-chain) linking it to the α4-helix (A-chain). For compounds **1–3**, the phenyl ring from cinnamaldehyde fragment is

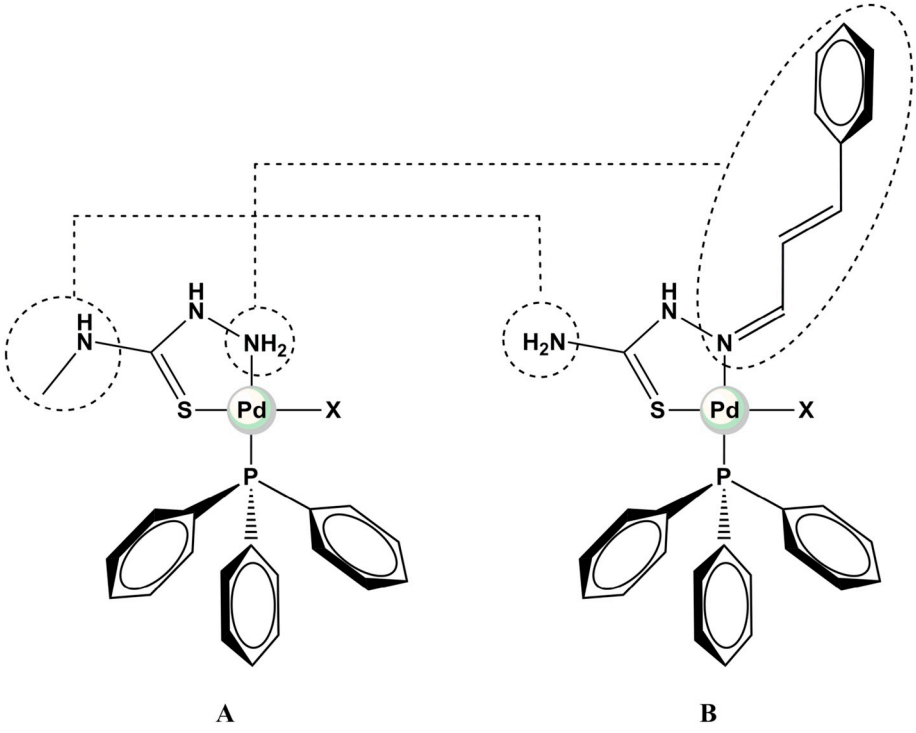

Fig. 2. (A) Molecular scaffold from hit-ligand (IC_{50} range 8.78–10.63 μM). (B) New designed Pd(II) compounds highlighting the incorporated cinnamaldehyde fragment at coordinating *N*-atom and H-donor group at *N*(4)-thiocarbamide position. X = Cl^-, I^-, NCS^-, N_3^- for **1–4**, respectively.

held in ANP-adenine ring site, which leads us to rationalize that thiosemicarbazone moiety increases the affinity in the hydrophobic pocket. The PPh_3 group establishes these conformations by hydrophobic interactions with side chains of K157 and V158 (Table 1, Fig. 4). The side chains of R98, E155 and E185 also contribute with hydrogen bond, π-cation and π-anion interactions concerning **1**, **2** and **4,** respectively. For that reason, the in silico evaluation suggested that **1–4** would act as TOP2A inhibitors by external modulation of the ATPase domain. Subsequently, all complexes have been synthesized.

Table 1
Computed interactions between key residues and the designed inhibitors on the ATPase domain. In the table, (*) and (+) mean hydrophobic and electrostatic interactions, respectively.

	Residues (TOP2A)							
Complex	R98	K123	P126	E155	K157	V158	E185	I406
1				(+)	(*)	(*)		
2	(+)				(*)			
3						(+)		
4	(+)	(*)	(*)		(*)		(+)	(*)

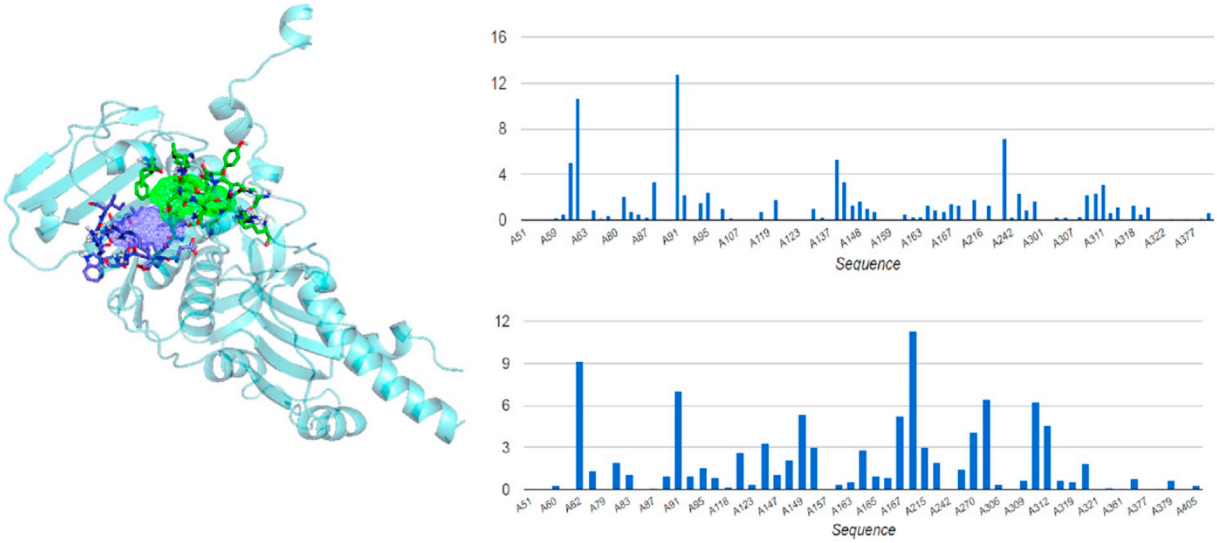

Fig. 3. On the left, the FT-map result for the ATPase domain of the 1ZXM.pdb (chain A). On the right, computed contribution of mean sidechain residues involved in intermolecular interactions with theoretical probes. Blue region has been classified as a hydrophobic pocket while the green region has been indicated as an electrostatic one.

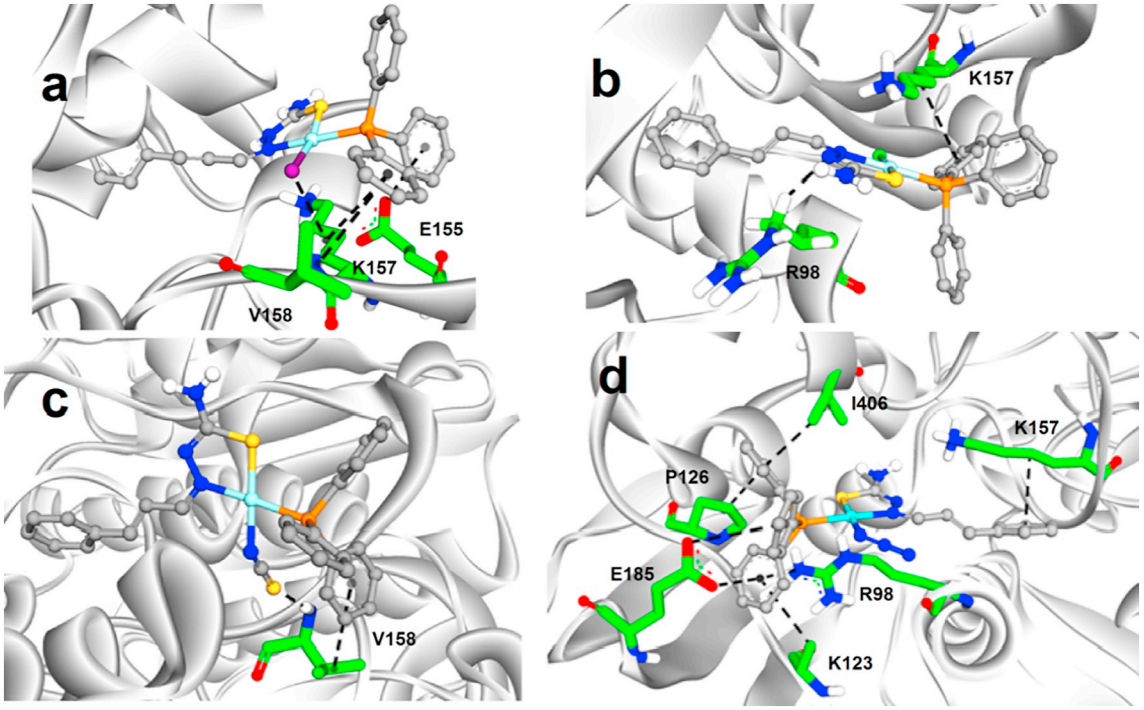

Fig. 4. The best docking pose of the **1–4** at the ATPase domain. The **1–4** molecules are a–d, respectively. The mean residues are shown in sticks style: carbon in green, oxygen in red and nitrogen in dark blue. All intermolecular interactions are shown as dashed black lines.

2.3. Chemistry

2.3.1. Synthesis and characterization comments

Concerning the synthesis (Scheme 1), the precursor $[PdCl_2(MeCN)_2]$ reacts with PPh_3 and (2*E*)-2-[(2*E*)-3-phenyl-1-ylidene]hydrazinecarbothioamide in chloroform/methanol (3:1) affording $[PdCl(PPh_3)(TSC)]$ **1**. Compounds $[PdI(PPh_3)(TSC)]I$ **2**, $[Pd(SCN)(PPh_3)(TSC)]$ **3** and $[PdN_3(PPh_3)(TSC)]$ **4** are readily obtained via metathesis of the coordinated chloride in **1** by iodide, thiocyanate and azide salts, respectively. For more details about experimental protocols, please see ESI.

Single crystals of **2** were acquired by slow vapor diffusion of hexane into a saturated chloroform solution and analyzed by means single crystal X-ray diffraction. Unfortunately, we failed to grow single crystals from compounds **1**, **3** and **4**.

The syntheses were carried out at room temperature with constant magnetic stirring. The complexes are air-stable powders and exhibit colour that varies from yellow to red. The compounds **1–4** are soluble in DMSO, DMF and $CHCl_3$, moderately soluble in CH_3CN, MeOH and EtOH, but insoluble in H_2O. The molar conductivities of complexes **1**, **3** and **4** in DMF were found between 9.5 and 28 $\Omega^{-1}\,cm^2\,mol^{-1}$, in agreement with their non-electrolytic nature [18–20]. Nonetheless, the

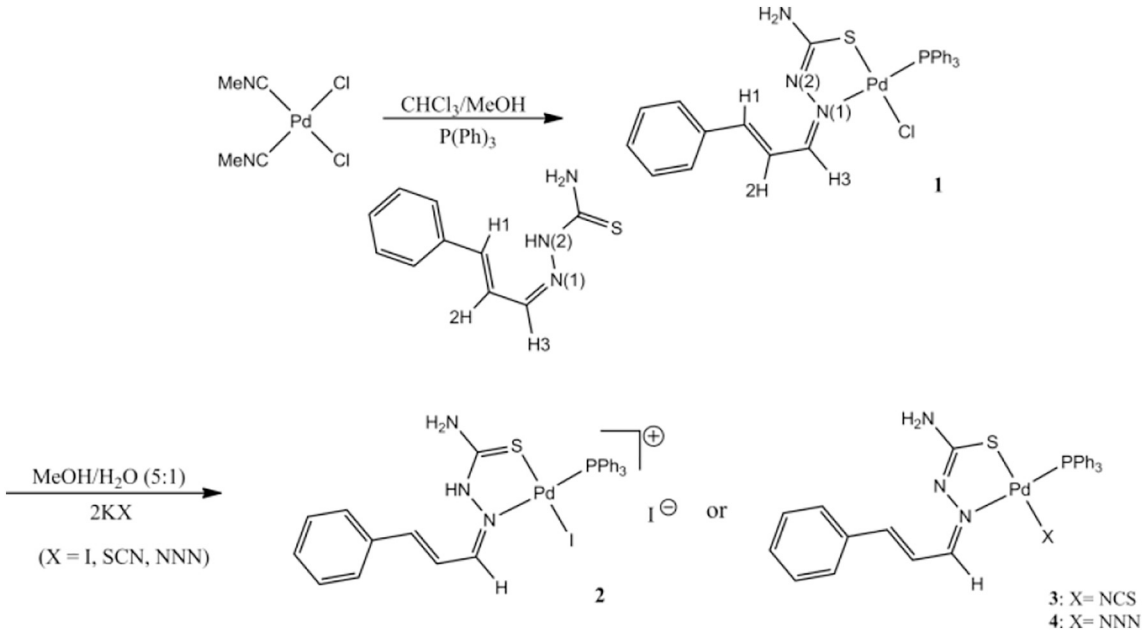

Scheme 1. Scheme of the reaction for compounds **1–4**.

molar conductivity of **2** appears as 46 Ω^{-1} cm^2 mol^{-1} suggesting a 1:1 ionic nature. The elemental analysis (CHN-%) results are in agreement with the proposed formulae (Table S1). The presence of $CHCl_3$ in the compounds **1** and **2** was supported by the appearance of its characteristic peak at 8.30 ppm in their respective ^{1}H NMR spectra ($CDCl_3$). The presence of the molecule of $CHCl_3$ was detected as disordered solvate in the asymmetric unit structure of **2**.

In order to confirm the composition of the new complexes, ES mass spectra were recorded in positive mode. The molecular ion peaks (M+) observed at m/z = 623, 714, 644 and 628 supporting the molecular formulae. In addition, representative fragment peak at 586 was observed in the spectra of all four complexes. This fragment indicated the complexes without the halide or pseudohalide ligands (Cl^-, I^-, NCS^- and N_3^-).

2.3.2. Spectroscopy

The vibrational bands of TSC and its complexes are reported in Table S2. Bands assigned to ν(CS) and ν(CN) modes are very useful to enlighten the coordination mode of TSC in compounds **1–4**. The infrared (IR) spectrum of free TSC exhibits a strong band at 1515 cm^{-1} corresponding to νC=N. Upon coordination, the νC=N band was shifted 45 cm^{-1} to a higher frequency in all IR spectra of the complexes indicating the participation of azomethine nitrogen in bonding [19,21]. A sharp band observed at 754 cm^{-1}, with a high contribution of νC=S mode in the TSC ligand, shifted to 708 cm^{-1} in the IR spectra of **1**, **3** and **4**, indicating the *S*-coordination and consequently the enolization followed by deprotonation of the thiosemicarbazone [19,21]. Furthermore, the characteristic bands ascribed to triphenylphosphine were present in the expected spectral region [22–25]. The terminal *N*-bonded coordination mode of the thiocyanate ligand in **3** was inferred by the presence of a sharp ν_{as}(NCS) band at 2087 cm^{-1} [26,27]. The azido ligand in **4** is terminally coordinated due to the presence of ν_{as}(NNN) band at 2037 cm^{-1}.

The ^{1}H nuclear magnetic resonance (^{1}H NMR) spectra of ligand and the four complexes were recorded in $CDCl_3$. Chemical shifts and assignments are summarized in Table S3. The ^{1}H NMR spectrum of the free ligand showed the expected signals and integrations. Although the overall pattern of the ^{1}H NMR spectra of **1–4** resemble closely to that of the free ligand [28], most of the signals have been shifted after coordination, such as those assigned to H1 (7.9–9.0 ppm), H2 (8.2–8.3 ppm) and H3 (7.2–7.4 ppm). In the ^{1}H NMR spectra of **1**, **3** and **4** the signals attributed to NH_2 group from thioamide moiety were hidden by the multiplet associated with aromatic protons. In addition, the disappearance of the signal ascribed to hydrazine N(2)HCS hydrogen reinforces the idea of deprotonation of thiosemicarbazone ligand in **1**, **3** and **4**. On the other hand, the thiosemicarbazone acts as a neutral k^2*N*,*S*-chelating ligand in **2** because of the presence and downfield shift of the N(2)HCS signal (13.1 ppm) together with the appearance of two signals ascribed to NH_2 at 6.1 and 9.2 ppm [19]. In all four complexes, a multiplet appeared at 7.3–7.8 ppm due to aromatic protons of the ligand and triphenylphosphine.

2.3.3. Crystal structure

The asymmetric unit of **2** consists of one Pd(II)-cationic complex entity, one iodide counter anion and one-half disordered $CHCl_3$ solvate molecule (Fig. 5). The Pd(II)-ion is fourfold coordinated in a distorted square-planar environment by one k^2*N*,*S*-chelating cinnamaldehyde-thiosemicarbazone, forming a five-membered metallaring, one PPh_3 and one terminal iodide ligands. The maximal deviation from the Pd1/I1/N3/S1/P1 plane amounts to 0.1027 (14) Å for N3 [root-mean-square deviation of fitted atoms = 0.0857 Å]. For the crystal structure details, see ESI.

2.4. Biological assays

2.4.1. Human Topoisomerase II inhibition assay

Agarose gel electrophoresis experiments have been performed to determine the in vitro TOP2A inhibitory activity for **1–4** (Fig. 6). Circular pBR322 plasmid DNA was incubated with the enzyme in the presence of 3.12, 6.25, 12.5 and 25.0 μM of the compounds.

Both **1** and **2** were able to inhibit TOP2A at 25 μM while compounds **3** and **4** could induce its inhibition at 12.5 and 6.25 μM, respectively. These data showed that **1–4** avoid relaxation of the supercoiled DNA in a lower concentration than some drugs whose have TOP2A as target (etoposide 35 μM and merbarone 40–50 μM) [29,30].

2.4.2. Resazurin cell viability activity

The cytotoxicity profile of free TSC ligand and **1–4** complexes was investigated on five tumor cell lines: MCF-7 and MDA-MB-231 (human breast), DU145 (human prostate), A549 (human lung) and Cal27 (human tongue). Three observations can be made from that: (1) The free TSC ligand showed no drug response at < 100 μM towards tested cultures, which highlights the importance of molecular scaffold provided by the metal coordination; (2) **1–4** exhibited better cytotoxicity than reported for cisplatin against MCF-7, MDA-MB-231 and DU-145, but the compounds were fewer actives for Cal27 and A549 cell lines [31–34]; (3) Non-largest difference in cytotoxic effects was observed among the complexes according to the anionic group, which lead us to consider non-influence of these (Tab. 2).

The development of compounds with selectivity for tumor cells rather than normal ones is a mandatory characteristic, nonetheless at the same time the major challenge in anticancer drug research. Thus, the selectivity index (SI) of **1–4** and cisplatin was evidenced performing comparative cytotoxicity between MCF-7 and non-tumor cell HEK-293 (human kidney), since MCF-7 was more sensitive cell line to action of the Pd(II)-derivatives and the nephrotoxicity is an important side effect associated with the use of cisplatin [35,36]. Outstandingly, **1–4** were more selective than cisplatin (see, Tab. 2), notably **2**, **3** and **4** that revealed SI of 3.65, 5.01 and 4.50, respectively. Many authors have considered that active compounds with SI value > 3.0 are recognized as very selective [32,37,38]. Herein, evaluated palladium compounds have displayed the ability to inhibit TOP2A functions at similar range from IC_{50}. Since MCF-7 tumor cells are well-known by their significant expression of TOP2A, the increased SI values for compounds **3** and **4** can be enlightened [39–41].

2.4.3. Red blood cells hemolytic test

In addition to selectivity, the study of concentration effect in toxicology is essential in order to assure the therapeutic index of active compounds. In this sense, the assessment of cytotoxicity through hemolytic tests has proved to be an efficient screening method [42,43]. Erythrocytes lysis may be photometrical monitored by measuring the released hemoglobin in the supernatants, whose concentration is directly proportional to the number of lysed human red blood cells (RBC). The degree of in vitro cytotoxicity to hemolytic activity is evaluated using the mortality rate observed: 0% to 9% = non-toxic; 10% to 49% = slightly toxic; 50% to 89% = toxic; and 90% to 100% = highly toxic [42,43]. The effects observed for **4**, the most promising TOP2A inhibitor, on RBC indicated hemolysis of 0.9, 3.3, 7.5, and 24% at concentrations of 3.12, 6.25, 12.5 and 25.0 μM, respectively[‡]. Thus, is possible asserts non-toxicity for **4** in molar concentration close to IC_{50} (2.98 ± 0.45 μM, Tab. 2) and slightly toxicity in a dose approximately 8-fold higher than one.

3. Conclusion

In summary, the computational methodology developed herein was appropriate to evaluate the preferred orientations for square-planar Pd (II) complexes at the ATPase domain. The changes performed over the molecular scaffold from hit-molecule resulted in allosteric inhibitors of the TOP2A. In addition, compounds **2**, **3** and **4** displayed significant selectivity against MCF-7 cells compared to normal HEK-293 cell line as well as good relationships between TOP2A inhibition and SI value was found. Finally, **4** appear as the most promising molecule, if we take into

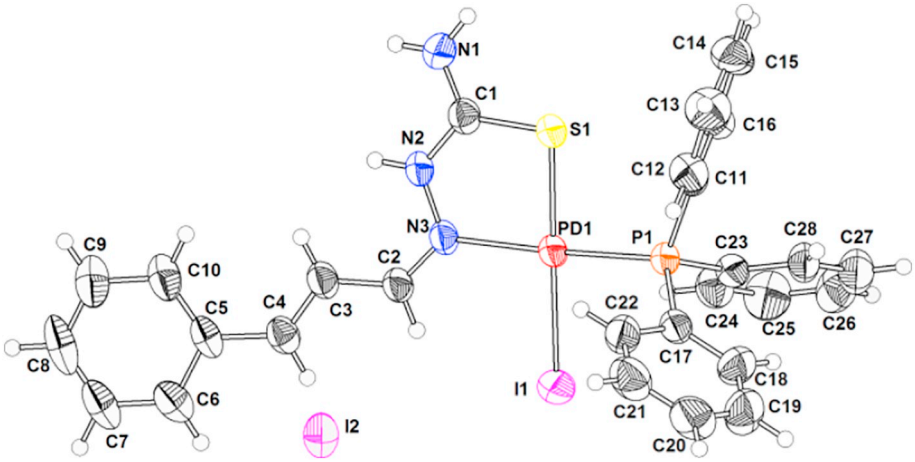

Fig. 5. The asymmetric unit of 2 and atom-labelling scheme, displacement ellipsoids are drawn at 50% probability level. The disordered chloroform molecule is not shown for clarity.

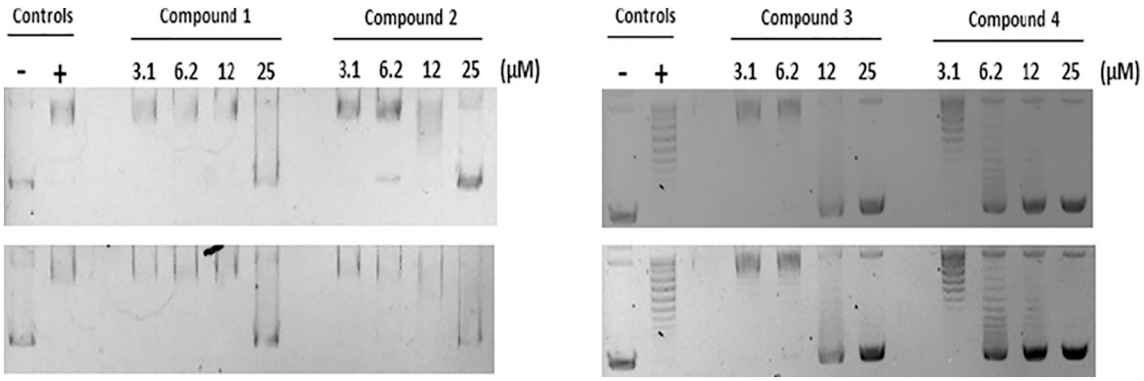

Fig. 6. Effects of the complexes **1–4** on the catalytic cycle of TOP2A, determined by relaxation assay. C– = Supercoiled DNA; C+ = DNA and TOP2A.

account its high cytotoxicity, selectivity and low hemolytic profile.

4. Theoretical and Experimental Protocols

4.1. In silico Simulation

4.1.1. Compounds construction and semi-empirical optimization

All molecular structures for designed complexes were generated with Discovery Studio Visualizer (DSV/Version: 17.2.0) [44]. They were optimized by using the semi-empirical method PM7 in MOPAC package (Version 2016) through the graphical interface software, Gabedit 2.5.0 [45]. Because of improbable distortion of the metallic centre from square-planar molecular geometry to tetrahedral, constraint was applied to coordinating *S*- and *N*-atoms by setting their scale factors from 1 to 0 in *.mop input. The commands used during optimization were: MMOK, GOE-OK, BFGS, XYZ, T = 10D, ALLVEC, SPARKLE, CHARGE = 0 (or +1, depending on the compound), PRECISE and SINGLET. The format of the optimized compound file was *.mol2. The 3-D heavy atom coordinate comparisons among two minimized compounds and respective crystallographic ones were made to verify the quality of the theoretical optimization, Fig. S1.

Table 2
IC_{50} and TOP2A inhibition results for complexes **1–4** and free TSC ligand.

	TSC	1	2	3	4	Cisplatin [31–34]
	IC_{50} (μM)					
MCF-7	> 100	4.46 ± 1.23	1.81 ± 0.85	2.69 ± 0.27	2.98 ± 0.45	19.6 ± 4.20
MDA-MB-231	> 100	6.42 ± 0.66	9.21 ± 0.24	6.02 ± 0.66	> 20	67.0 ± 1.06
DU-145	> 100	6.47 ± 0.51	9.62 ± 0.81	5.01 ± 0.24	15.42 ± 1.75	15.0 ± 1.40
A549	> 100	> 20	> 20	> 20	> 20	4.97 ± 0.32
Cal27	> 100	7.55 ± 1.21	5.66 ± 0.95	10.90 ± 1.14	7.22 ± 0.61	3.11 ± 1.07
HEK-293	> 100	6.20 ± 0.83	6.61 ± 0.78	13.48 ± 1.32	13.41 ± 1.17	2.42 ± 0.65
SI	Nd	1.4	3.6	5.0	4.5	0.12
TOP2A	Nd	[a]	[a]	[b]	[c]	Nd

[+] 25 μM.
[++] 12.5 μM.
[+++] 6.2 μM.

4.1.2. Protein Crystallographic Structure Assessment and Docking Methodology

The 3-D file (*.pdb) from Human DNA Topoisomerase II-α was obtained from Protein Data Bank (PDB ID: 1ZXM), which display X-ray resolution of 1.87 Å. Afterwards, the protein structure quality was evaluated after uploading it on RAMPAGE web server to analyse the Ramachandran plot (Fig. S2a) [46]. Subsequently, the missing residues were built in Swiss-PDB Viewer software (v4.1.0) [47]. The CHARMm force field in DSV was used to correct the φ and Ψ angles of the outlier residues, as observed in the Ramachandran Plot. This improved protein structure was resubmitted to RAMPAGE to verify correction of the φ and Ψ angles (Fig. S2b). ProSA-web was used to check the Z-score quality parameter (Fig. S3) [48]. The feature and key residues of the ATPase-binding site were mapped into FT-site and FT-map webservers (Fig. 3) [49]. The binding site was set to be the same as for the crystallized ANP ligand, which was also set as reference. In sequence, by using GOLD software (Version v5.5) [50], the 1ZXM coordinates were uploaded. In order to preserve the position of the atoms obtained by X-ray diffraction, the rigid molecular docking was performed. Previously, the water molecules were removed; docking radius was set as 20 Å and 50 docking poses were set to each ligand. The following parameters were exploited to identify the best docking conditions: four high-performance scoring functions (ASP, ChemScore, ChemPLP and GoldScore) were analyzed. Each parameter was evaluated based on the root-mean-square deviation of the top-ranked redocked pose referenced to the original atom positions from ANP ligand in the crystal structure (Fig. S4). Finally, the fit solutions for the Pd-compounds were analyzed through the best scoring function. The comparison of results is shown on a table containing the compounds and residues involved in protein-ligand interactions (see, Table 1 and Fig. 4).

4.2. General Methods

Reagents and solvents were purchased as reagent-grade from Acros, Sigma–Aldrich, and Fisher Scientific and used without further purification. NMR spectra were recorded in Fourier transform mode with a Bruker Fourier 300 spectrometer at 298 K. Residual solvent signals were used as internal references. Electrospray (positive mode) mass spectra were recorded with AB SCiex 3200 QTRAP equipment. Conductivities were measured with a Digimed-DM-31 conductometer using 1×10^{-3} mol L^{-1} solutions in DMF. IR spectra were recorded with a Perkin–Elmer Spectrum 200 spectrometer in the range 4000–400 cm^{-1} by using KBr pellets. Elemental analyses were performed with a Perkin Elmer 2400 series II.

4.3. Synthesis of Pd(II) complexes

[PdCl(PPh_3)(TSC)] (**1**): Triphenylphosphine (51.0 mg, 0.193 mmol) and (2*E*)-2-[(2*E*)-3-phenyl-1-ylidene] hydrazinecarbothioamide (TSC) (43.0 mg, 0.193 mmol) were treated with [$PdCl_2(MeCN)_2$] (50.0 mg, 0.193 mmol) in chloroform/methanol (10:2, v/v, 15 mL). After magnetic stirring for 2 h, the solvent was evaporated under reduced pressure to a final volume of ca. 5 mL. This resulting yellow solution was added to pentane (ca. 30 mL). The dark-yellow solid formed was filtered out, washed with chloroform/methanol (1:1), and finally dried under vacuum. Yield: 75%. Anal. Calc. [PdCl(PPh_3)(TSC)].$CHCl_3$: C 50.40, H 4.23, N 6.19%; Found C 50.80, H 4.17, N 6,19%. Key bands from FTIR $\nu(cm^{-1})$: 3248 $\nu_{as}(NH_2)$, 3258 $\nu_s(NH_2)$, 1618 $\delta(NH_2)$, 1592 ν(CC), 1561 [δ(NH) + ν(C=N)] (Thioamide I), 1435 [ν(C=N) + δ(NH) + δ(CH)] (Thioamide II), 999 ν(N=C) + ν(C=S) (thioamide III). ^{1}H NMR ($CDCl_3$) δ(ppm): 13.0 (s, 1H, NH), 7.83–7.44 (*m*, H_{ar}), 7.37 (d, 1H, H1), 8.22 (*dd*, 1H, H2), 8.42 (d, 1H, H3). ^{31}P NMR (dmso-d6) δ(ppm): 30.81.

[PdI(PPh_3)(TSC)]I (**2**): Triphenylphosphine (51.0 mg, 0.193 mmol) and TSC (43.0 mg, 0.193 mmol) were treated with [$PdCl_2(MeCN)_2$] (50.0 mg, 0.193 mmol) in chloroform/methanol (10:2, v/v, 15 mL). After 2 h, potassium iodide (64.0 mg, 0.386 mmol) in methanol/water (5:1, v/v, 3 mL) was added. The reaction mixture was magnetically stirred for 2 h, and then the solvent was evaporated under reduced pressure to give a final volume of ca. 5 mL and filtered. This resulting red solution was added to pentane (ca. 30 mL). A red solid formed was filtered out, washed with chloroform/methanol (1:1) and water. Finally, it was dried under vacuum yielding 70%. Suitable single crystals of 2 were acquired by slow vapor diffusion of hexane into a saturated chloroform solution and analyzed by means single crystal X-ray diffraction. Anal. Calc. [PdI(PPh_3)(TSC)]I.0.5$CHCl_3$: C 38.57, H 3.01, N 4.73%; Found C 38.89, H 2.92, N 4,82%. Key bands from FTIR $\nu(cm^{-1})$: 3426 ν(NH), 3235 $\nu_{as}(NH_2)$, 1612 $\delta(NH_2)$, 1590 ν(CC), 1560 [δ(NH) + ν(C=N)] (Thioamide I), 1435 [ν(C=N) + δ(NH) + δ(CH)] (Thioamide II), 997 ν(N=C) + ν(C=S) (thioamide III). ^{1}H NMR ($CDCl_3$) δ(ppm): 9.24/6.13 (s, 2H, NH_2), 7.83–7.44 (*m*, H_{ar}), 7.43 (d, 1H, H1), 8.23 (*dd*, 1H, H2), 8.99 (d, 1H, H3). ^{31}P NMR (dmso-d6) δ(ppm): 30.98.

[Pd(NCS)(PPh_3)(TSC)] (**3**): Prepared as described for 2 by the reaction of [$PdCl_2(MeCN)_2$] (50.0 mg,0.193 mmol) with triphenylphosphine (51.0 mg, 0.193 mmol), TSC(43.0 mg, 0.193 mmol), and potassium thiocyanate (38.0 mg, 0.386 mmol) to yield 72% of complex 3 as a light-orange solid. Anal. Calc. [Pd(NCS)(PPh_3)(TSC)]: C 54.35, H 4.39, N 8.88%; Found C 54.68, H 4.08, N 8,51%. Key bands from FTIR $\nu(cm^{-1})$: 3306 $\nu_{as}(NH_2)$, 3165 $\nu_s(NH_2)$, 2087 ν_{as}(NCS), 1607 $\delta(NH_2)$, 1590 ν(CC), 1560 [δ(NH) + ν(C=N)] (Thioamide I), 1435 [ν(C=N) + δ(NH) + δ(CH)] (Thioamide II), 999 ν(N=C) + ν(C=S) (thioamide III). ^{1}H NMR ($CDCl_3$) δ(ppm): 7.72–7.38 (*m*, H_{ar}), 7.21 (d, 1H, H1), 8.87 (d, 1H, H3). ^{31}P NMR (dmso-d6) δ(ppm): 26.36.

[Pd(NNN)(PPh_3)(TSC)] (**4**): Prepared as described for 2 by the reaction of [PdCl2(MeCN)2] (50.0 mg,0.193 mmol) with triphenylphosphine (51.0 mg, 0.193 mmol), TSC(43.0 mg, 0.193 mmol), and potassium azide (31.0 mg, 0.386 mmol) to yield 60% of complex 4 as a yellow solid. Anal. Calc. [Pd(NCS)(PPh_3)(TSC)]: C 54.68, H 4.10, N 13.67%; Found C 54.80, H 4.16, N 13,29%. Key bands from FTIR $\nu(cm^{-1})$: 3347 $\nu_{as}(NH_2)$, 3177 $\nu_s(NH_2)$, 2037 ν_{as}(NNN), 1608 $\delta(NH_2)$, 1590 ν(CC), 1560 [δ(NH) + ν(C=N)] (Thioamide I), 1435 [ν(C=N) + δ(NH) + δ(CH)] (Thioamide II), 999 ν(N=C) + ν(C=S) (thioamide III). ^{1}H NMR ($CDCl_3$) δ(ppm): 7.78–7.39 (*m*, H_{ar}), 7.21 (d, 1H, H1), 8.42 (d, 1H, H3). ^{31}P NMR (dmso-d6) δ(ppm): 27.20.

4.4. Biological assays

4.4.1. Resazurin cell viability assay

The cell viability correlates with cell ability to reduce Resazurin [51]. Briefly, the cells (3.0×10^3 cells/well) were cultured in 96-well plates and incubated with the compounds for 48 h in different concentrations (6.25 μM, 12.5 μM, 25.0 μM, 50.0 μM, 100.0 μM, 150.0 μM and 200.0 μM). After incubation, the medium was replaced by DMEM medium without phenol red (SIGMA) and added resazurin (0.01 mg mL^{-1}; SIGMA) dissolved in PBS and kept protected from light for up to 4 h in an incubator. The reading was held in a microplate fluorimeter (excitation 530/25 nm, emission 590/35 nm). A blank control and positive control were included in all experiments. All assays were performed in triplicate. The IC_{50} value was estimated using a non-linear regression algorithm.

4.4.2. Statistical analysis

The statistical analyses and graphics were done with GraphPad Prism 5 for Windows [52]. The statistical test used was the ANOVA, Dunnett's posttest and the level of significance was set at $p < 0.05$.

4.4.3. Human Topoisomerase II inhibition assay

Human Topoisomerase II relaxation kit was purchased of the Inspiralis Limited. Reaction mixture (30 mL) contained 10 mM Tris.HCl (pH 7.9), 50 mM NaCl, 50 mM KCl, 5.0 mM $MgCl_2$, 0.1 mM Na_2H_2EDTA, 15 mg mL^{-1} BSA, 1.0 mM ATP, 500 ng pBR322 DNA, 4.0

nmolL^{-1} Topo II, and different concentrations of complexes. The reaction mixtures were incubated at 37 °C for 1 h, and the reaction was finished by the addition of 3 mL SDS, 15 mL of STEB and 60 mL of chloroform: isoamyl alcohol (24:1 v/v) mixture, centrifuged and analyzed. The samples were electrophoresed at 60 V for 2 h and the gel was stained with ethidium bromide solution (1 mg mL^{-1}) and analyzed by an Alpha Imager EP System of Alpha Innotech.

4.4.4. Hemolytic profiles

The hemolytic activities of the synthesized compounds were determined on human red blood cells. Human blood from healthy individuals was collected in tubes containing EDTA as an anticoagulant. The erythrocytes were harvested by centrifugation for 10 min at 2.000 rpm, followed by washing three times with Phosphate buffered saline (PBS, pH 7.4, 8.5 mg mL^{-1}). PBS was added to the pellet, to yield a 10% (v/v) erythrocytes/PBS suspension. The 10% suspension was then diluted to 1:10 in PBS. From each suspension, 100 µL was added to 100 µL of different dilution series of synthesized compounds in the same buffer in Eppendorf tubes (in triplicate). Total hemolysis was achieved with 1% Triton X-100. The tubes were incubated for 1 h at 37 °C and then centrifuged for 10 min at 2.000 rpm. From the supernatant fluid, 50 µL was transferred to a 96 wells plate, and the absorbance was measured spectrophotometrically at 540 nm in a Microplate Spectrophotometer Epoch-Biotek. The hemolysis percentage was calculated by the following equation:

$$\%Hemolise = \frac{A_{540}\ of\ compound\ test\ treat\ sample - A_{540}\ of\ buffer\ treat\ sample}{A_{540}\ of\ 1\%triton - X\ treat\ sample - A_{540}\ of\ buffer\ treat\ sample}$$

Abbreviations

A	Alanine
A549	Human lung cancer cells
ANP	adenosine-5′-(b,c-imido)triphosphate
ATP	Adenosine triphosphate
Cal27	Human tongue cancer cells
ChemPLP	GOLD fitness scoring function
D	Aspartate
DNA	Deoxyribonucleic acid
DU-145	Human prostate cancer cells
E	Glutamate
EtOH	Ethanol
F	Phenylalanine
G	Glycine
GHKL	Histidine kinase, DNA gyrase B and HSP90 ATPase domains.
HEK-293	Human normal kidney cells (embryonic)
I	Isoleucine
K	Lysine
MCF-7	Human breast cancer cells
MDA-MB-231	Human breast cancer cells
MeCN	Acetonitrile
MeOH	Methanol
N	Asparagine
PDB	Protein Data Bank
PM7	Semi-empirical Parametric Method 7
PPh_3	Triphenylphosphine
Q	Glutamine
R	Arginine
RBC	human red blood cell
S	Serine
SI	selectivity index
TCZ	Thiosemicarbazide
TOP1	Human Topoisomerase I
TOP2A	Human Topoisomerase Iiα
TOP2B	Human Topoisomerase Iiβ
TSC	Thiosemicarbazone
V	Valine
Y	Tyrosine

Notes

Crystallographic supplementary data can be accessed in the Cambridge Structural Database (CCDC Number 1873138). This study was approved by the Research Human Ethics Board of São Paulo State University (UNESP) (review number 1.185.001). There are no conflicts of interest to declare.

Acknowledgements

This work was sponsored by grants from FAPESP (proc. 2012/15486-3, 2013/20156-5, 2016/17711-5 and 2016/04201-9), CNPq INCT-INOFAR (proc. 573.564/2008-6), FAPERJ (proc. E-26/170.020/2008), PROPe-UNESP (proc. 840) and CAPES (Finance Code 001).

Appendix A. Supplementary data

Supplementary data to this article can be found online at https://doi.org/10.1016/j.jinorgbio.2019.110725.

References

[1] J.L. Nitiss, Nat. Rev. Cancer 9 (2009) 338–350.
[2] Y. Pommier, ACS Chem. Biol. 8 (2013) 82–95.
[3] G. Dong, Y. Wu, Y. Sun, N. Liu, S. Wu, W.N. Zhang, C. Sheng, MedChemComm 9 (2018) 1142–1146.
[4] P.-H. Li, P. Zeng, S.-B. Chen, P.-F. Yao, Y.-W. Mai, J.-H. Tan, T.-M. Ou, S.-L. Huang, D. Li, L.-Q. Gu, Z.-S. Huang, J. Med. Chem. 59 (2016) 238–252.
[5] Y.L. Lyu, J.E. Kerrigan, C.-P. Lin, A.M. Azarova, Y.-C. Tsai, Y. Ban, L.F. Liu, Cancer Res. 67 (2007) 8839.
[6] K.J. Kilpin, P.J. Dyson, Chem. Sci. 4 (2013) 1410–1419.
[7] B.M. Zeglis, V. Divilov, J.S. Lewis, J. Med. Chem. 54 (2011) 2391–2398.
[8] F. Bisceglie, A. Musiari, S. Pinelli, R. Alinovi, I. Menozzi, E. Polverini, P. Tarasconi, M. Tavone, G. Pelosi, J. Inorg. Biochem. 152 (2015) 10–19.
[9] F.V. Rocha, C.V. Barra, S.S. Garrido, F.A. Manente, I.Z. Carlos, J. Ellena, A.S. Fuentes, A. Gautier, L. Morel, A.E. Mauro, A.V. Netto, J. Inorg. Biochem. 159 (2016) 165–168.
[10] H. Wei, A.J. Ruthenburg, S.K. Bechis, G.L. Verdine, J. Biol. Chem. 280 (2005) 37041–37047.
[11] F. Bisceglie, S. Pinelli, R. Alinovi, M. Goldoni, A. Mutti, A. Camerini, L. Piola, P. Tarasconi, G. Pelosi, J. Inorg. Biochem. 140 (2014) 111–125.
[12] J.J. Stewart, J. Mol. Model. 19 (2013) 1–32.
[13] D. Kozakov, D.R. Hall, G.-Y. Chuang, R. Cencic, R. Brenke, L.E. Grove, D. Beglov, J. Pelletier, A. Whitty, S. Vajda, Proc. Natl. Acad. Sci. 108 (2011) 13528–13533.
[14] Y.-C. Chen, Trends Pharmacol. Sci. 36 (2015) 78–95.
[15] R. Dutta, M. Inouye, Trends Biochem. Sci. 25 (2000) 24–28.
[16] C.H. Douse, S. Bloor, Y. Liu, M. Shamin, I.A. Tchasovnikarova, R.T. Timms, P.J. Lehner, Y. Modis, Nat. Commun. 9 (2018) 651.
[17] L. Neckers, B. Blagg, T. Haystead, J.B. Trepel, L. Whitesell, D. Picard, Cell Stress and Chaperones 4 (2018) 467–482.
[18] H.B.A.D. Gambino, Mini-Rev. Med. Chem. 4 (2004) 31–39.
[19] T.S. Lobana, R. Sharma, G. Bawa, S. Khanna, Coord. Chem. Rev. 253 (2009) 977–1055.
[20] V.G. Rand, E. Lisic, FASEB J. 30 (2016) 612.615.
[21] K.S.O. Ferraz, N.F. Silva, J.G. Da Silva, N.L. Speziali, I.C. Mendes, H. Beraldo, J. Mol. Struct. 1008 (2012) 102–107.
[22] F.J. Ramos-Lima, A.G. Quiroga, B. García-Serrelde, F. Blanco, A. Carnero, C. Navarro-Ranninger, J. Med. Chem. 50 (2007) 2194–2199.
[23] F.V. Rocha, C.V. Barra, A.E. Mauro, I.Z. Carlos, L. Nauton, M. El Ghozzi, A. Gautier, L. Morel, A.V.G. Netto, Eur. J. Inorg. Chem. 2013 (2013) 4499–4505.
[24] C. da Silva, J.G. Ferreira, A.E. Mauro, R.C.G. Frem, R.H.A. Santos, P.B. da Silva, F.R. Pavan, L.B. Marino, C.Q.F. Leite, A.V.G. Netto, Inorg. Chem. Commun. 48 (2014) 153–155.
[25] C. da Silva, L.B. Ribeiro, C.C. Furuno, G.A. da Cunha, R.F.F. de Souza, A.V.G. Netto, A.E. Mauro, R.C.G. Frem, J.A. Fernandes, F.A. Almeida Paz, L.B. Marino, F.R. Pavan, C.Q.F. Leite, Polyhedron 100 (2015) 10–16.
[26] T.R. de Moura, S.L. Cavalcanti, P.R.D.V. de Godoy, E.T. Sakamoto-Hojo, F.V. Rocha, E.T. de Almeida, V.M. Deflon, A.E. Mauro, A.V.G. Netto, Transit. Met. Chem. 42 (2017) 565–574.
[27] J.L. Burmeister, F. Basolo, Inorg. Chem. 3 (1964) 1587–1593.
[28] J. Liu, R. Cao, W. Yi, C. Ma, Y. Wan, B. Zhou, L. Ma, H. Song, Eur. J. Med. Chem. 44 (2009) 1773–1778.

[29] F. Gao, H. Chao, L.N. Ji, Chem. Biodivers. 5 (2008) 1962–1979.
[30] J.M. Fortune, N. Osheroff, J. Biol. Chem. 273 (1998) 17643–17650.
[31] F. Shahsavar, M. Bozorgmehr, E. Mirzadegan, A. Abedi, Z.M. Lighvan, F. Mohammadi, N. Safari, V. Amani, A. Zarnani, Anti Cancer Agents Med. Chem. 16 (2016) 393–403.
[32] C. Dai, J. Li, P. Chen, H. Jiang, M. Wu and Y. Chen, J. Biomed. Sci. 22 (2015) 77.
[33] U. Kotowski, g. Heiduschka, m. Brunner, b.M. Erovic, h. Martinek, d. Thurnher, Oncol. Lett. 3 (2012) 1326–1330.
[34] H. Katsuda, M. Yamashita, H. Katsura, J. Yu, Y. Wki, N. Nagata, Y. Sai, K. Miyamoto, Biol. Pharm. Bull. 33 (2010) 1867–1871.
[35] E.d.O. Lopes, C.G. de Oliveira, P.B. da Silva, C.E. Eismann, C.A. Suárez, A.A. Menegário, C.Q.F. Leite, V.M. Deflon, F.R. Pavan, Int. J. Mol. Sci. 17 (2016) 781.
[36] R.P. Miller, R.K. Tadagavadi, G. Ramesh, W.B. Reeves, Toxins 2 (2010) 2490–2518.
[37] W. Mahavorasirikul, V. Viyanant, W. Chaijaroenkul, A. Itharat, K. Na-Bangchang, BMC Complement. Altern. Med. 10 (2010) 55.
[38] M.P. Chelopo, S.A. Pawar, M.K. Sokhela, T. Govender, H.G. Kruger, G.E. Maguire, Eur. J. Med. Chem. 66 (2013) 407–414.
[39] G. MacGrogan, P. Rudolph, I. Mascarel Id, L. Mauriac, M. Durand, A. Avril, J.M. Dilhuydy, J. Robert, S. Mathoulin-Pélissier, V. Picot, A. Floquet, G. Sierankowski, J.M. Coindre, Br. J. Cancer 89 (2003) 666–671.
[40] V. Durbecq, M. Paesmans, F. Cardoso, C. Desmedt, A. Di Leo, S. Chan, K. Friedrichs, T. Pinter, S. Van Belle, E. Murray, I. Bodrogi, E. Walpole, B. Lesperance, S. Korec, J. Crown, P. Simmonds, T.J. Perren, J.Y. Leroy, G. Rouas, C. Sotiriou, M. Piccart, D. Larsimont, Mol. Cancer Ther. 3 (2004) 1207–1214.
[41] M. Martin-Richard, M. Muñoz, J. Albanell, L. Colomo, M. Bellet, M.J. Rey, J. Tabernero, C. Alonso, A. Cardesa, P. Gascon, P.L. Fernandez, Oncology 66 (2004) 388–394.
[42] M. Pagano, C. Faggio, Cell Biochem. Funct. 33 (2015) 351–355.
[43] J. V. C. Orsine, R. V. da Costa, R. C. da Silva, M. d. F. M. A. Santos and M. R. C. G. Novaes, International Journal of Nutrition and Metabolism, 2012, 4, 19-23.
[44] H. Kemmish, M. Fasnacht, L. Yan, PLoS One 12 (2017) e0177923.
[45] A.R. Allouche, J. Comput. Chem. 32 (2010) 174–182.
[46] S.C. Lovell, I.W. Davis, W.B. Arendall, P.I. de Bakker, J.M. Word, M.G. Prisant, J.S. Richardson, D.C. Richardson, Proteins 50 (2003) 437–450.
[47] M.U. Johansson, V. Zoete, O. Michielin, N. Guex, BMC Bioinformatics 13 (2012) 173.
[48] M. Wiederstein, M.J. Sippl, Nucleic Acids Res. 35 (2007) W407–W410.
[49] D. Kozakov, L.E. Grove, D.R. Hall, T. Bohnuud, S.E. Mottarella, L. Luo, B. Xia, D. Beglov, S. Vajda, Nat. Protoc. 10 (2015) 733.
[50] Y.-C. Chen, Trends Pharmacol. Sci. 36 (2015) 78–95.
[51] J. O'Brien, I. Wilson, T. Orton, F. Pognan, Eur. J. Biochem. 267 (2000) 5421–5426.
[52] D.R. Appling, J. Am. Chem. Soc. 130 (2008) 6056.